FIN BUFFET CHARACTERISTICS OF ADVANCED TRAINER AIRCRAFT

Christian Breitsamter, Arne Schmid, Jan-Ulrich Klar, and Roman Reß
Institute of Aerodynamics, Technische Universität München
Boltzmannstrasse 15, D-85748 Garching, Germany

Keywords: *Vortex flows, high agility aircraft, fin buffet, unsteady aerodynamic loads*

Abstract

The present study focuses on the characteristics of the vortical flow field emanating from a wing-strake configuration and associated buffet loads experienced on the vertical tail (fin). The wind tunnel configuration studied is a single fin high-agility trainer aircraft with a 45 deg swept trapezoidal wing, wing strakes at air intakes and horizontal tail plane. The results presented include turbulent flow fields based on advanced hot-wire anemometry as well as unsteady fin pressures measured with surface embedded miniature sensors. The tests are conducted in the low-speed region at a Reynolds number of $Re_{l\mu} \approx 0.7 \times 10^6$ for angles of attack of $\alpha = 0$ deg to $\alpha = 30$ deg. The fin flow field is dominated by large-scale vortices shed already at low angles of attack at the leading-edges of wing and strakes. Bursting of the leading-edge vortices over the wing starts already at $\alpha \approx 5$ deg. The associated regions of highly turbulent flow increase in their spatial extension and intensities with increasing angle of attack. A significant rise in the fluctuations of flow velocities and fin surface pressures above a certain angle of attack is a characteristic feature of the fin buffet flow. The fluctuations show narrow-band spectral energy distributions related to the helical mode instability of the breakdown flow. The induced un-steady loads may strongly excite the fin in its structural eigenmodes. The results demonstrate that the corresponding unsteady aerodynamic loads must be carefully addressed in the design process.

1 Introduction

The flight envelope of high maneuverable aircraft is limited by dynamic aeroelastic problems including buffeting, buzz and flutter [1-3]. Many efforts have been spend on the fin buffeting problem because it is a critical issue for high performance fighter aircraft limiting the maximum angle of attack. Fin buffeting became a major problem for many configurations fitted with twin vertical tails [4-7]. Also, single fin aircraft are affected, especially at sideslip [8, 9]. The corresponding unsteady aerodynamic loads occur mainly at high angles of attack and are caused by the highly turbulent flow due to burst leading-edge vortices. Generally, strong large-scale vortices dominate the suction side of slender wing geometries at angle of attack, in particular, considering delta wings, strakes or leading-edge extensions [10, 11].

The evolution and development of leading-edge vortices depend on wing sweep and angle of attack. The related vortex topologies can be divided into four ranges [12]: The first range is linked to a *partly developed* leading-edge vortex. As roll-up of the separating shear layer starts at the wing rear part, the vortex is only present along a rearward portion of the leading-edge at very low angles of attack. The forward part shows attached flow and/or a separation bubble. The shear layer roll-up progresses rapidly to the apex with increasing angle of attack or wing sweep. Consequently, vorticity feeding exists along the entire leading-edge. This vortical flow type is related to the second range designating the *fully developed* leading-edge vortex. The vortex strength increases with angle

of attack while the vortex axis moves inboard and upward. This fully developed, stable vortex improves significantly maneuver capabilities because of additional lift and an increase in maximum angle of attack. The transition from range one to range two depends on the presence of a laminar or turbulent boundary layer [13]. For a given wing sweep, the laminar boundary layer creates the fully developed vortex at a lower angle of attack relative to the turbulent case. The third range marks the case of the *spanwise fixed* leading-edge vortex. Due to the mutually lateral blockage of the port and starboard vortex, the vortex axis can only move upward if the angle of attack is further increased. The transition from range two to range three depends again on whether a laminar or turbulent boundary layer is present. The spanwise fixed vortex occurs only for a wing sweep larger than 65 deg. The fourth range is attributed to the stage of *vortex bursting* or vortex breakdown revealing itself as a sudden massive expansion of the vortex core flow [14, 15]. This expansion is caused by the adverse pressure gradient which increases with angle of attack leading to a stagnation of the axial core flow at a certain incidence. A substantial decrease of the vortex induced velocities results. Bursting starts over the wing at the trailing–edge and the breakdown position moves forward with further raising the angle of attack. Thus, the wing upper surface is more and more affected by the breakdown flow, the suction level becomes diminished and the lift coefficient decreases. For Reynolds numbers of $Re > 10^4$ and typical leading-edge vortex swirl numbers, vortex breakdown is of the spiral type [14]. At moderate wing sweep, burst leading-edge vortices exist over a large incidence range until the maximum angle of attack is reached. These leading–edge vortex topologies determine markedly the aircraft maneuverability at moderate and high angles of attack.

The breakdown flow leads to high turbulence levels and specific instability mechanisms resulting in narrow-band unsteady aerodynamic forces [6, 16, 17]. The predominant phenomena are sketched in Fig. 1, [12]. The corresponding dynamic loads often excite the vertical tail structure in its natural frequencies causing

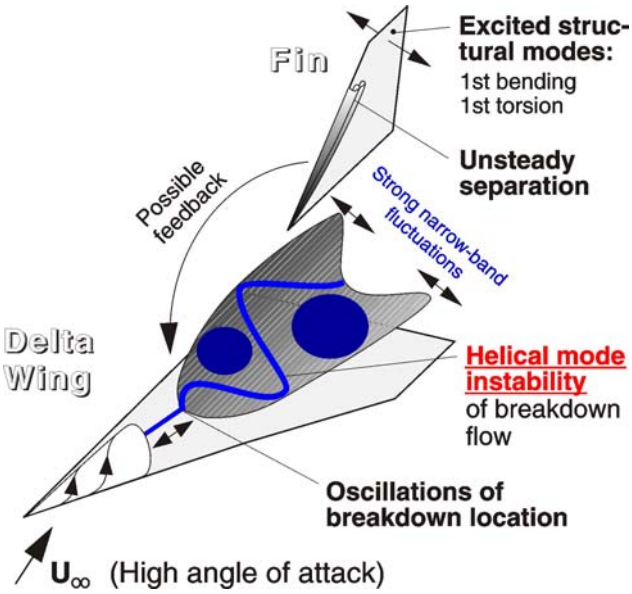

Fig. 1 Phenomenology of fin buffeting induced by the flow of burst leading-edge vortices [12].

increased fatigue loads [2]. Service life is reduced and maintenance costs increase. Therefore, comprehensive studies concentrate on the fin buffeting problem including methods of flow control [18-20] and aerodynamic and structural means of active vibration alleviation [21-25].

Unsteady vortex structures develop also at moderately swept wings studied here for the configuration of a typical light combat / advanced trainer aircraft. The present investigation analyses the fin unsteady aerodynamic loads as well as the turbulent flow fields creating such loads.

2 Wind Tunnel Testing

2.1 Model and Facility

Experiments are performed on an 1:15 scaled detailed steel model of a high performance trainer aircraft of wing-strake type (Fig. 2a). Major parts of the model include front fuselage and canopy, center fuselage with swept trapezoidal wing, air intake strakes and a through-flow double air intake, and rear fuselage including nozzle section and horizontal and vertical tail (fin). The leading-edge sweep of wing, intake strakes and horizontal tail plane is 45 deg.

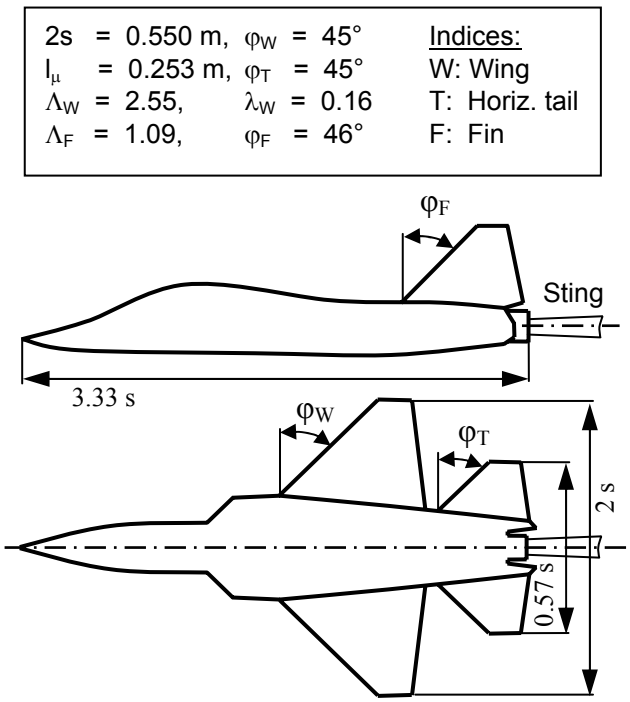

a) Geometry and reference quantities

b) Model mounted in the test section; α = 0°.

c) Model mounted in the test section; α = 25°.

Fig. 2 Wind tunnel model of advanced trainer aircraft.

The measurements have been carried out in the low-speed wind tunnel facility B of the Institute of Aerodynamics of the Technische Universität München. This closed-return wind tunnel is operated with an open test section at maximum usable velocity of 60 *m/s*. Test section dimensions are 1.2 *m* in height, 1.55 *m* in width and 2.8 *m* in length. The test section flow has been carefully inspected and calibrated documenting a turbulence level less than 0.4% and uncertainties in the spatial and temporal mean velocity distributions of less than 0.067%. The maximum blockage at the model incidence of $\alpha = 30°$ is about 5%.

The model is sting mounted using a tail sting connected to the horizontal sting of the 3-axis model support (Figs. 2b, c). The computer controlled model support provides an angle-of-attack range of $-10° \leq \alpha \leq +30°$, and models may be yawed and rolled 360°. The uncertainty in angle setting is less than 0.05°.

2.2 Experimental Set-up and Test Conditions

Mean velocities and turbulence quantities are measured applying advanced hot-wire anemometry. Unsteady fin surface pressures are recorded by means of miniature transient pressure transducers. The model fin is instrumented with 3 differential unsteady pressure transducers (Fig. 3). The sensor voltages of each channel are amplified for optimal signal levels, low-pass filtered at 256 *Hz* and sampled with 2000 *Hz*. The data of all channels are acquired simultaneously over a time interval of 15 *sec*. and digitized with 14 bit precision. The signal resolution is about 2 *Pa*.

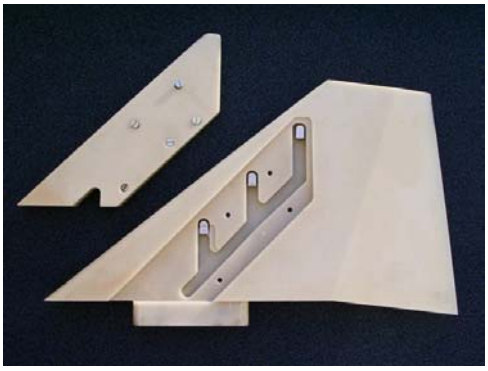

Fig. 3 Fin with instrumentation cover.

The time dependent flow field velocities are measured using advanced hot-wire anemometry. A three-axes traversing system moves a miniature cross-wire probe to the points of the cross-flow plane located at the fin position (Fig. 3). The measurement points are equally spaced in lateral and vertical direction with a relative distance based on the wing semi span *s* of 0.036. Thus, the number of survey points is approximately 650 for each angle of attack. The anemometer output voltages are low-pass filtered at 1000 *Hz* and sampled with 3000 *Hz* over 6.4 *sec*. The digital resolution is 16 bit. The data acquisition parameters are based on preliminary tests to ensure that all relevant flow field phenomena are captured as well as on statistical accuracies of 1%, and 2.5% for the root mean square (rms) values and spectral densities, respecttively.

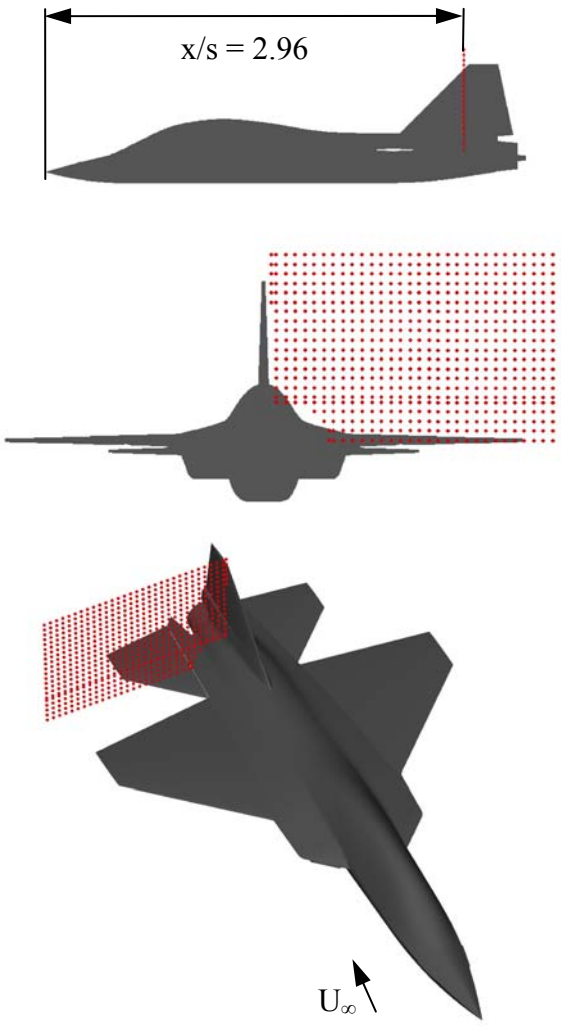

Fig. 3 Location of measured cross-flow plane and resolution of measurement grid.

The measurements have been made at a free stream reference velocity of U_∞ = 40 *m/s* at ambient pressure p_∞ and ambient temperature T_∞. The corresponding Reynolds numbers based on the wing mean aerodynamic chord l_μ is $Re_{l\mu}$ = 0.68 x 10^6 (M_∞ = 0.12). Turbulent boundary layers are present at wing and control surfaces for the angles of attack of interest. All control surfaces, namely leading- and trailing-edge flaps and horizontal tail plane are set to 0°. Flow field surveys are conducted at angles of attack of α = 10°, 15°, 20°, 25° and 30°, while fin pressure fluctuations are taken in the range of 0° $\leq \alpha \leq$ 30° with the following incidence steps: 0° $\leq \alpha \leq$ 10°: $\Delta\alpha$ = 5°; 10° $< \alpha \leq$ 20°: $\Delta\alpha$ = 2°; 20° $< \alpha \leq$ 30°: $\Delta\alpha$ = 1° .

3 Results and Discussion

The analysis of the fin buffet flow environment is based on field distributions of mean velocities and vorticities and turbulence intensities. The development of such field patterns with increasing angle of attack highlights the flow field impact on the fin.

3.1 Steady Fin Flow Field

Mean axial vorticity ξ (Fig. 4) and mean axial velocity $\bar{u}/U_\infty$ (Fig. 5) distributions are used to give a general overview of the vortex dominated flow field in the fin region. The quantities are shown in non-dimensional form referring to free stream velocity U_∞ and semi span *s* respectively;

$$\xi = (d\bar{w}/dy - d\bar{v}/dz)\cdot(s/U_\infty)$$

The flow field of the measurement plane is characterized by the presence and interaction of several vortex systems, mainly produced by the wing and the air intake wing strake (Fig. 4a). The main vortices are the wing leading-edge vortex, the wing tip vortex and the strake vortex linked to areas of radial distributed vorticity of elliptical shape. This vorticity pattern together with the deficit (20% – 40%) in the axial core velocities clearly indicates the presence of burst leading-edge vortices (Fig. 5a). For this wing planform, bursting of the wing leading-edge vortex starts with vortex formation already at $\alpha \approx 5°$.

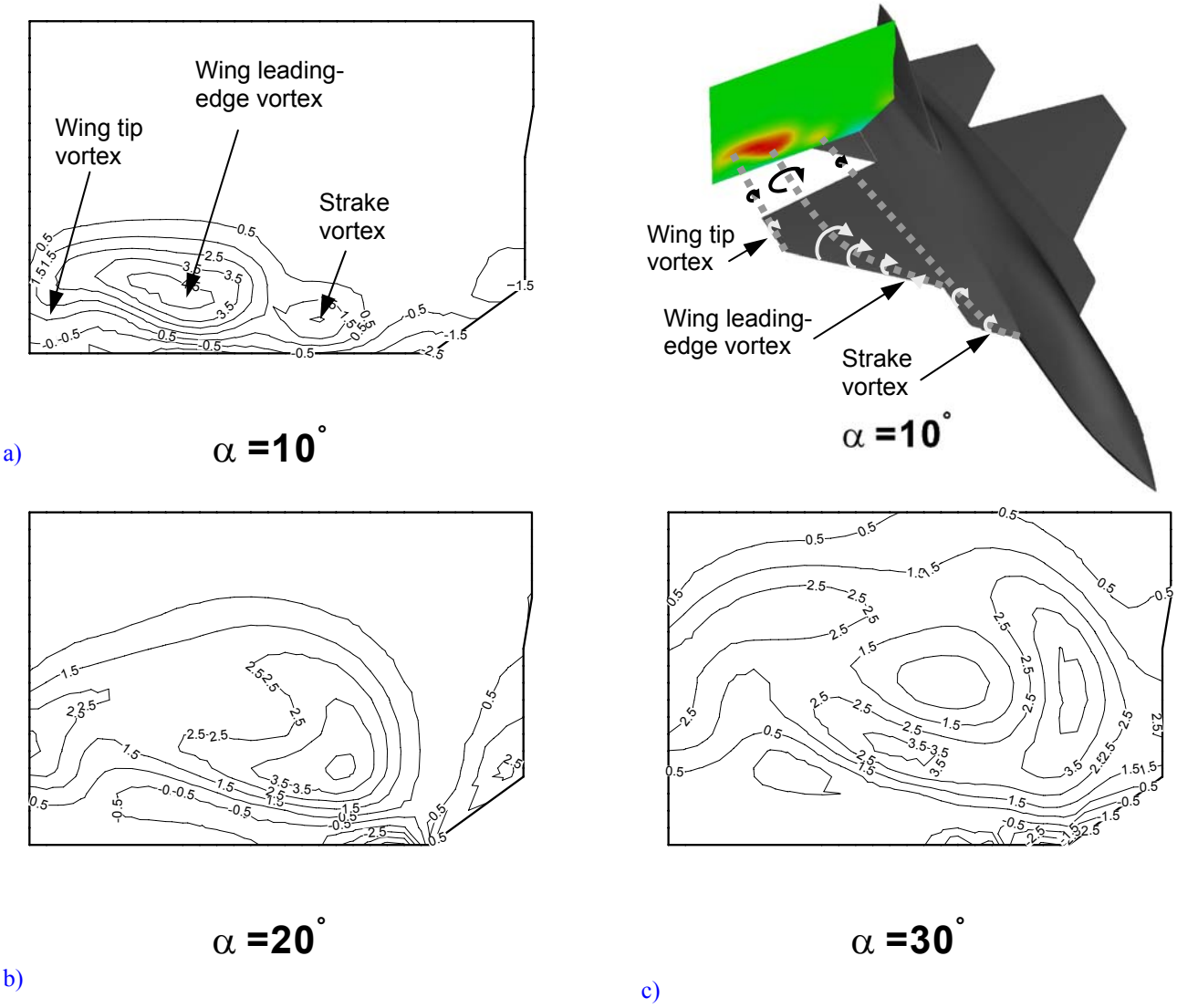

Fig. 4 Non-dimensional axial vorticity distributions ξ at α = 10°, 20°, and 30°; U_∞ = 40 m/s, $Re_{l\mu} \approx 0.7 \times 10^6$.

The wing leading-edge vortices move inboard towards the fuselage and upward above the wing with increasing angle of attack (Figs. 4b, 5b, c). The area of axial peak vorticities is also shifted inboard due to the merging of the wing leading-edge vortex with the strake vortex. The maxima of axial velocity deficits as well as the corresponding elliptical region increase significantly reflecting the strong expansion of the burst vortex core. Thus, the shear layer surrounding the vortex core area exhibits a strong axial velocity gradient. The inboard region of large velocity gradients is shifted towards the centerline fin when further raising the angle of attack. Above α = 20°, the distance between the outer shear layer of the burst vortex core and the symmetry plane becomes smaller than the core radius. The axial flow is moderately accelerated along the spanwise direction in the area under the burst vortex which detaches from the wing surface. At high angle of attack, the burst wing leading-edge vortex increases further in its radial extension associated with a further enlargement of the core area (Fig. 4c, Figs. 5d, e). Although the core region of reduced axial velocity comprises nearly 80% of the wing semi span, a structured swirling flow pattern can be observed around it. Axial peak vorticities are still concentrated on an inboard area where the burst wing and strake vortices are linked. Small regions of negative axial vorticity occur at the fuselage junction because of the negative

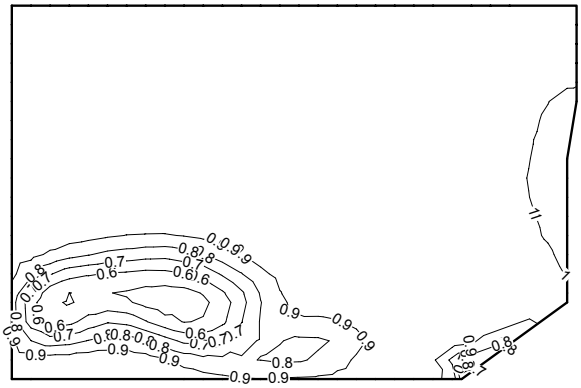

a) $\alpha = 10^{\circ}$

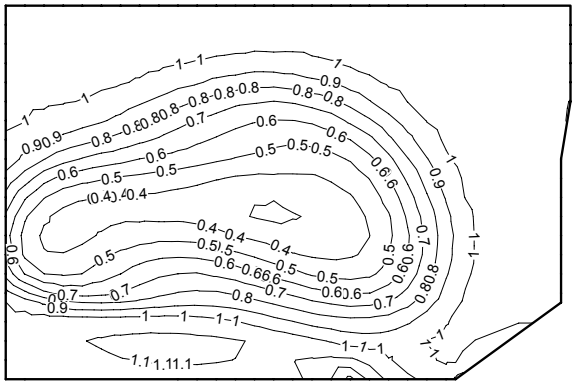

d) $\alpha = 25^{\circ}$

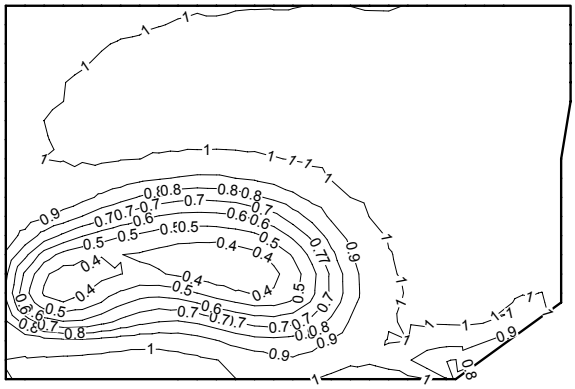

b) $\alpha = 15^{\circ}$

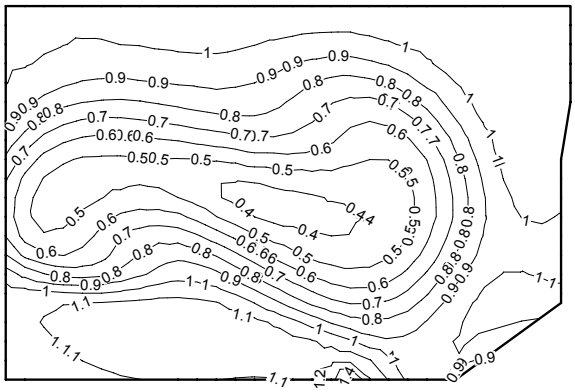

e) $\alpha = 30^{\circ}$

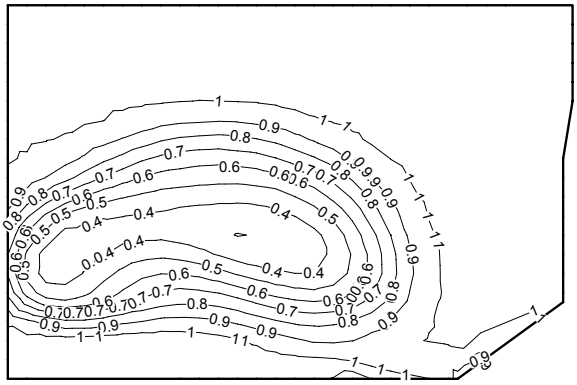

c) $\alpha = 20^{\circ}$

Fig. 5 Axial velocity distributions $\overline{u}/U_{\infty}$ at α = 10°, 15°, 20°, 25° and 30°; U_{∞} = 40 m/s, $Re_{l\mu} \approx 0.7 \times 10^{6}$.

circulation gradient towards the fuselage.

3.2 Turbulent Fin Flow Field

3.2.1 Axial and lateral velocity fluctuations

The turbulent flow structure is discussed using the root mean square (rms) values of the velocity fluctuations in axial and lateral direction, *u'* and *v'*, normalized with the free stream velocity U_{∞}: $u_{rms}/U_{\infty} = \sqrt{\overline{u'^2}}/U_{\infty}; v_{rms}/U_{\infty} = \sqrt{\overline{v'^2}}/U_{\infty}$.

The vortex regions are linked to areas of inreased velocity fluctuations. The burst wing leading-edge vortex creates a spanwise elliptical zone of high turbulence intensities where the local maxima are concentrated within a limited

radial range (Fig. 6a). This annular structure of local turbulence maxima is a characteristic feature of spiral vortex breakdown, documented also by many other investigations [12, 17]. The local turbulence maxima correspond to the points of large inflections in the radial profiles of the retarded axial core flow. Large velocity gradients and curvatures in the velocity profiles are due to the shear layer of the remaining swirling flow pattern surrounding the burst vortex core, as discussed above. There is a strongly expanded inner part of the burst vortex core characterized by very low velocity magnitudes and small velocity gradients, thus reducing the turbulence levels in this inner core region. The strake vortex reveals itself by a circle-like area of increased rms velocities which is already connected to the inboard wing vortex shear layer.

The turbulent regions grow considerably in both size and strength when increasing the angle of attack (Figs. 6b, c, d). This growth is caused by the radial expansion of the burst wing vortex core, the axis of which is shifted inboard and upwards. Therefore, the turbulent region attributed to the strake vortex becomes completely embedded in the limited radial range of turbulence maxima of the burst wing vortex. The maxima of the rms velocity fluctuations reach levels up to 28% (Fig. 6e). The inboard area of maximum turbulence levels approaches the symmetry plane at high angle of attack so that neighboured flow regions are strongly influenced by induction effects. At $\alpha = 30°$, nearly the entire measurement plane is dominated by very large velocity fluctuations.

The impact of the flow field on the fin structure can be quantified by the lateral rms velocities, v_{rms}, obtained in detail within the fin region (Figs. 7, 8). Summarizing, the lateral rms values are shown for a leading-edge position near the fin tip as function of angle of attack in Fig. 8. In addition, Fig. 7 presents lateral rms velocity patterns for the cross-flow plane aligned normal to the fin, and for the fin plane itself. The analysis substantiates that the magnitude of the lateral rms velocities in the fin plane depends on the development of the wing vortex systems observed in the cross-flow plane. At moderate angle of attack, the area of the centerline fin is only little affected by the regions of the highly turbulent flow associated with the burst wing leading-edge vortex and strake vortex. Above $\alpha = 20°$, a steep rise in the lateral velocity fluctuations starts induced by the inboard turbulence region approaching the mid-section (Fig. 8). Figs. 7b-d show that there are two areas of absolute fluctuation maxima within the annular range of local turbulence maxima increasing in size and intensity with increasing angle of attack. These turbulence areas reflect the interaction of wing and strake vortices, with the inboard turbulence area evoked by the strake vortex. The cross flow velocities of the wing vortex move the strake vortex downward while the expansion of the burst wing vortex causes an inboard shift of the strake vortex. At high angle of attack the strake vortex is further combined with a forebody vortex.

The induction of the turbulence region of the strake vortex leads to an axial area of local fluctuation maxima in the fin plane placed along the entire root chord (Fig. 7e). This effect becomes dominant for $\alpha > 20°$, and the fin area of local turbulence maxima increases in size and intensity with increasing angle of attack (Figs. 7f-h). Simultaneously, there is a shift from the fin root to the fin mid section reflecting the strake vortex expansion. Thus, the levels of the lateral rms velocities in the fin region reach approximately 6% of the free stream velocity at $\alpha = 30°$ (Fig 8). Because of the growth of the burst vortex cores with increasing incidence, a centerline fin may also encounter considerable turbulence levels at high angle of attack, while the turbulence intensities in the fin region can reach very high levels for a sideslip case. The latter may be comparable to those levels typically gained at twin-fin stations.

3.2.2 Spectral densities

The power spectral densities of the lateral velocity fluctuations $PSD_{v'}$ are plotted as function of frequency f and reduced frequency $k = fl_\mu/U_\infty$ (Fig. 9). Detailed formulas are given in Ref. 9. The frequency range is limited by the low-pass filter frequency of 1000 Hz set by the anemometer signal conditioner unit to meet the

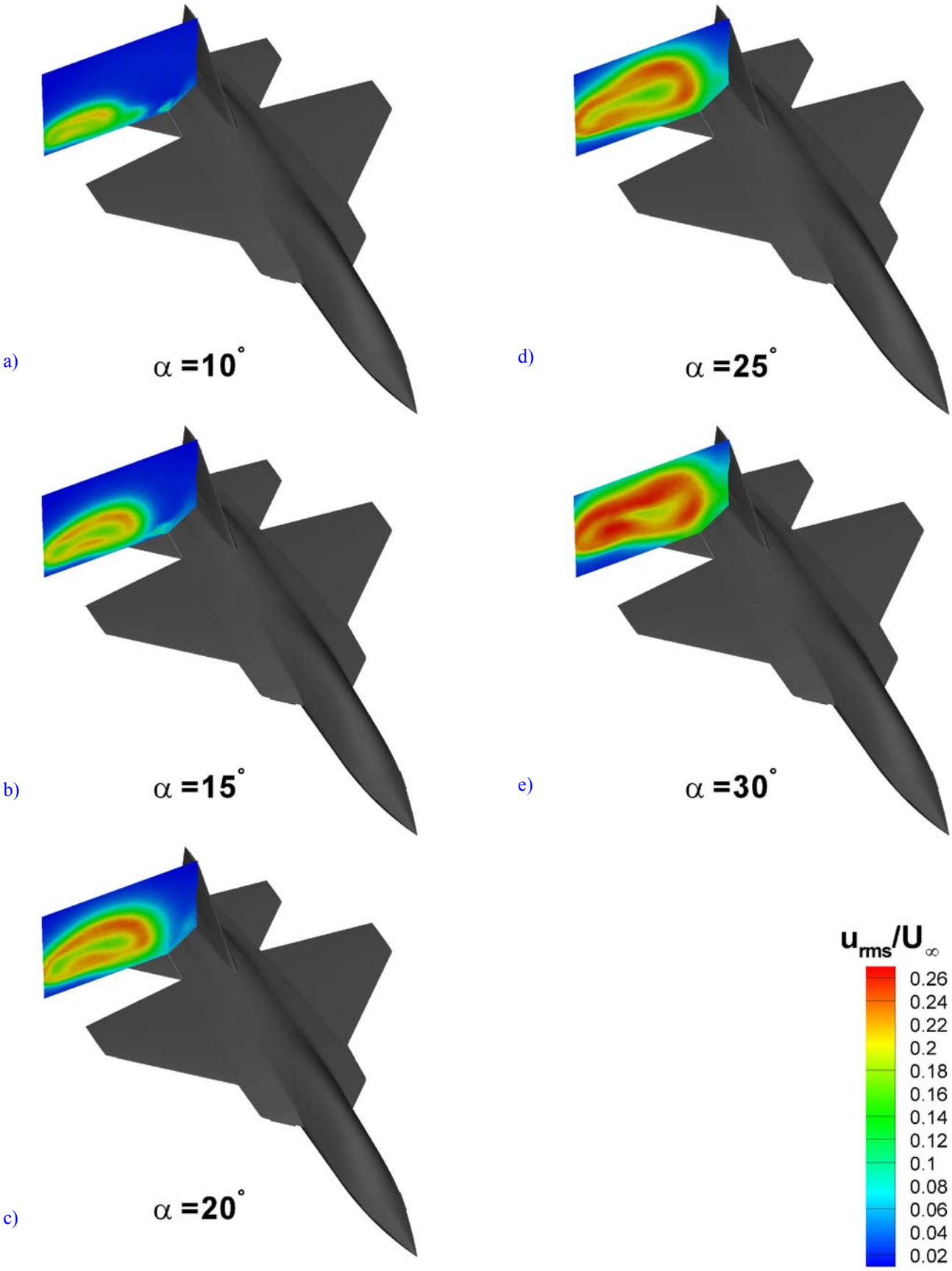

Fig. 6 Axial turbulence intensity distributions u_{rms}/U_∞ for $\alpha = 10°, 15°, 20°, 25°$ and $30°$; $Re_{l\mu} \approx 0.7 \times 10^6$.

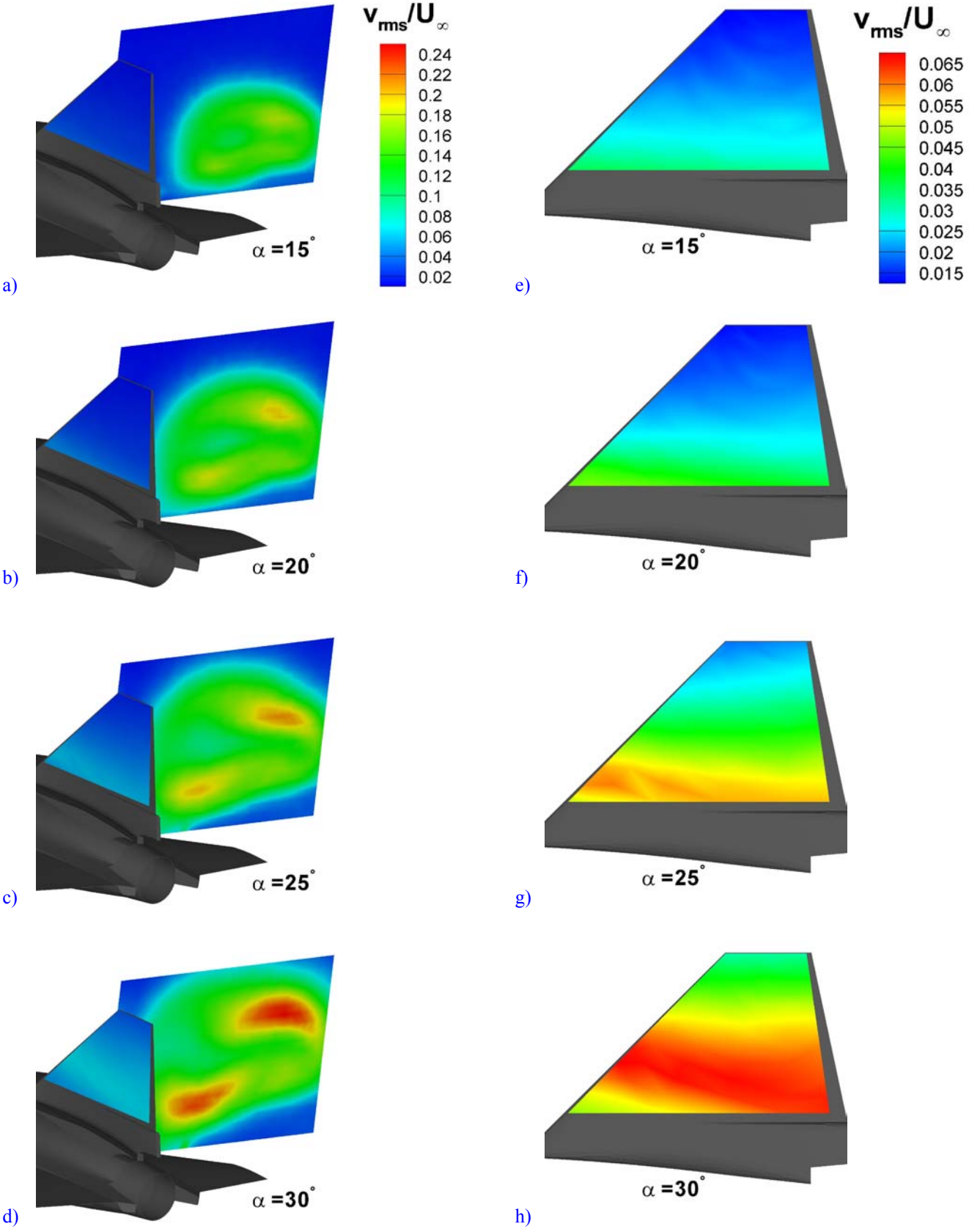

Fig. 7 Lateral turbulence intensity distributions v_{rms}/U_∞ for the plane normal to the fin and within the fin section at $\alpha = 15°, 20°, 25°$ and $30°$; $U_\infty = 40$ m/s, $Re_{l\mu} \approx 0.7 \times 10^6$.

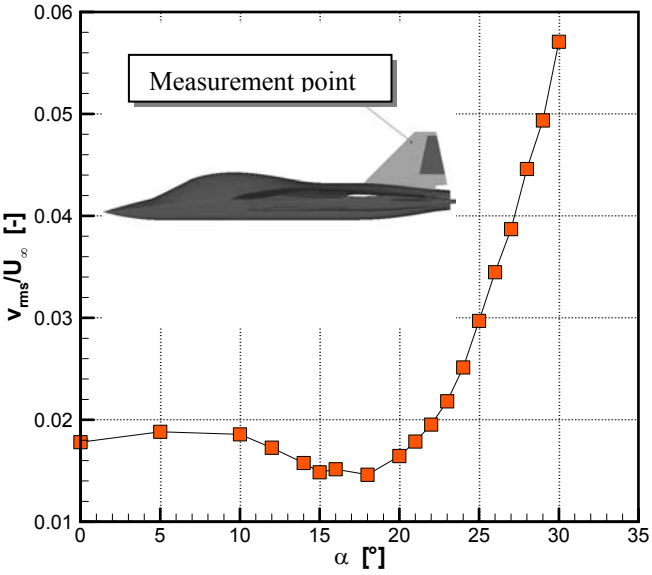

Fig. 8 Lateral rms velocities v_{rms}/U_∞ as function of angle of attack measured at a fin leading-edge tip station; $U_\infty = 40$ m/s, $Re_{l\mu} \approx 0.7 \times 10^6$.

Nyquist criterion (Nyquist freq.: 1500 Hz), Sec. 2.2. Analyzing the spectral content of the lateral velocity fluctuations it is shown that the flow downstream of vortex bursting exhibits a significant spectral peak indicating that turbulent kinetic energy is channeled into a narrow band (Figs. 9a-c). The frequency of this spectral peak is named "dominant frequency", f_{dom}.

The concentration of turbulent kinetic energy within a certain frequency range is linked to a specific instability mechanism, namely the helical mode instability of the breakdown flow [16, 17]. Consequently, quasi–periodic aerodynamic loads result which could strongly excite structural modes [6].

3.3 Unsteady Fin Surface Pressures

3.3.1 Buffet pressures

The unsteady flow field induces unsteady pressures on the fin defining the buffet situation. The rms values of the fluctuations in the pressure coefficient are plotted as function of angle of attack (Fig. 10). Results are shown for the three transducers, P1, P2 and P3. The unsteady fin surface pressures increase markedly above α = 20°, starting from a value of about 2% and reaching a level of about 9% - 10% at maximum angle of attack of α ≈ 30°. Generally the rms

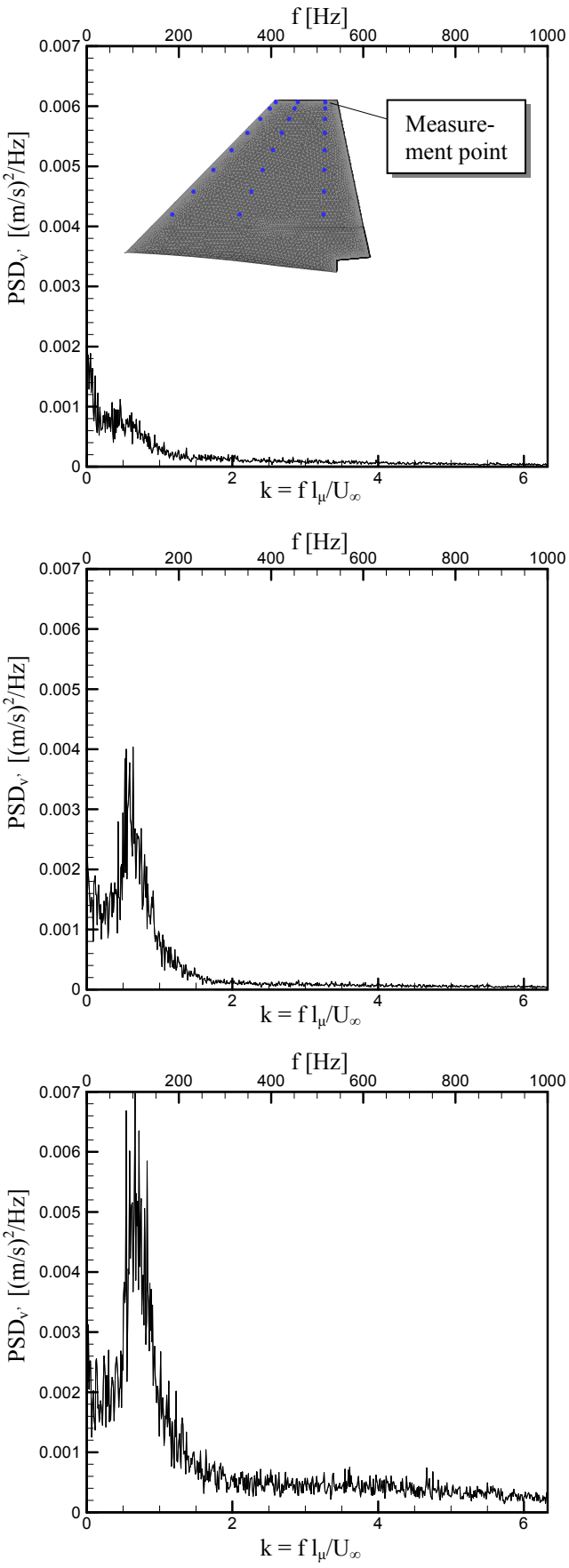

Fig. 9 Power spectral densities of the lateral velocity fluctuations $PSD_{v'}$ taken at a fin trailing-edge tip station for α = 15°, 20°, 25° and 30°; $Re_{l\mu} \approx 0.7 \times 10^6$.

curves reflect the trend in the lateral turbulence intensities (cp. Fig. 8). The severe increase in the rms pressures above a certain angle of attack is a characteristic feature of the fin buffet phenomenon.

3.3.1 Buffet spectra

The amplitude spectra of the fluctuating pressure coefficient $S_{Cp'}$, calculated from the signal taken at sensor station P1, are presented in Fig. 11 for several high angles of attack. Above $\alpha \approx 22°$, spectral peaks can be identified in the range of reduced frequencies of $k = 0.5 - 0.9$ ($k = f\,l_\mu / U_\infty$). It shows that the helical mode instability of the burst wing vortices starts to influence the fin pressure field. This induction evokes a strong rise in the narrow–band amplitude with increasing angle of attack from $\alpha = 22°$ to $\alpha = 30°$. The amplitude spectra further indicates that there is a frequency shift of the dominant spectral peak to lower frequency values raising the incidence. The burst vortex core expands with increasing angle of attack and, therefore, the wavelength of the instability mode becomes larger and the corresponding frequency smaller.

A universal frequency parameter k^*_{dom} can be derived using appropriate scaling quantities. Referring to velocity, the relevant component is the one normal to the leading–edge ($U_\infty \sin\alpha$). The characteristic length scale must account for the expansion of the burst leading–edge vortex core given approximately by the (local) semi span ($\sim s = c_r \cot\varphi_W$; c_r: root chord) and the distance between the inboard shear layers of the leading-edge vortices ($\sim \sin^2\alpha$). Using these relations results in a scaling with the sinus of the angle of attack and the co-tangent of the wing leading–edge sweep [12]:

$$k^*_{dom} = \frac{f_{dom} c_r \sin^2\alpha \cot\varphi_W}{U_\infty \sin\alpha} = \qquad (1)$$

$$= \frac{f_{dom} c_r}{U_\infty} \cot\varphi_W \sin\alpha = 0.28 \pm 0.05$$

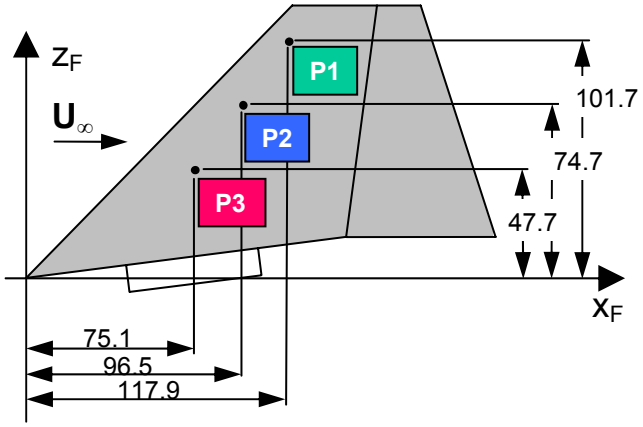

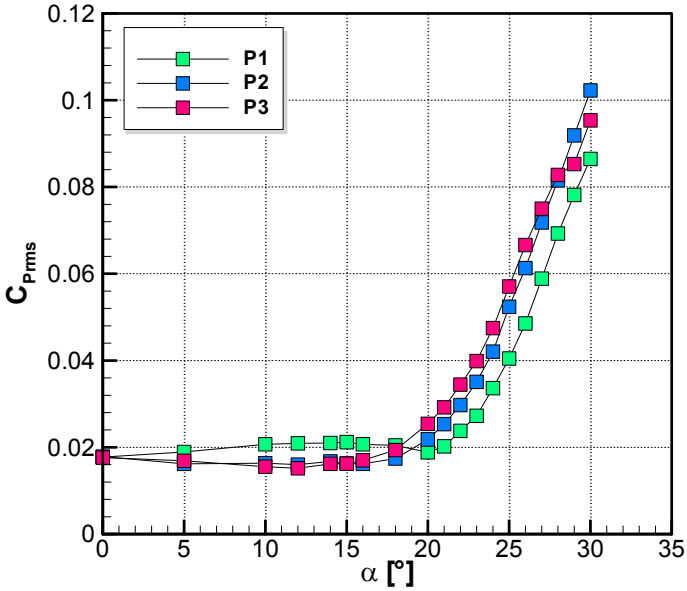

Fig. 10 Fin rms pressures as function of angle of attack; $U_\infty = 40$ m/s, $Re_{l\mu} \approx 0.7 \times 10^6$.

A comparison of the amplitude spectra of the three transducers at $\alpha = 28°$ shows a very similar spectral content (Fig. 12). The differences in the amplitude values are due to the inboard turbulence region associated with the shear layer of the burst wing vortex and the embedded strake vortex. This region of maximum fluctuations causes an induction which is the largest on the fin in the area where transducer P2 is located. There, the distance between the wing vortex shear layer and the fin surface is the smallest (cp. Figs. 7d, h).

Such pressure distributions create the buffeting, or structural response to the buffet. The resulting fin buffeting consists typically of a response in the first bending and torsion mode as shown in several studies [2, 6].

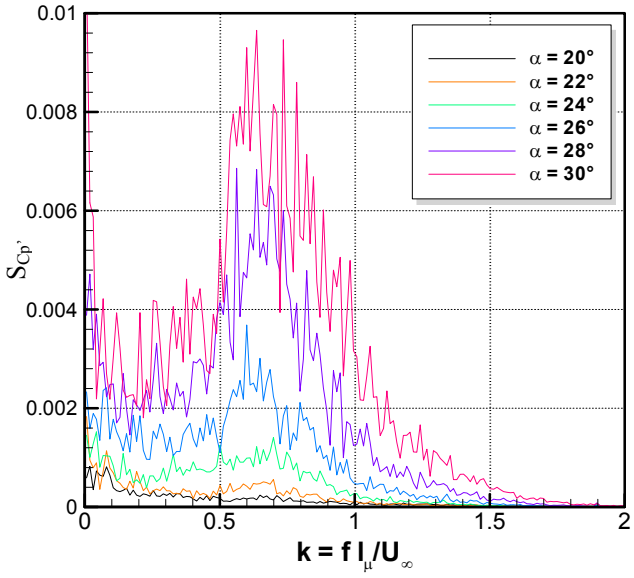

Fig. 11 Amplitude pressure spectra $S_{Cp'}$ taken at station P1 for several high angles of attack; $Re_{l\mu} \approx 0.7 \times 10^6$.

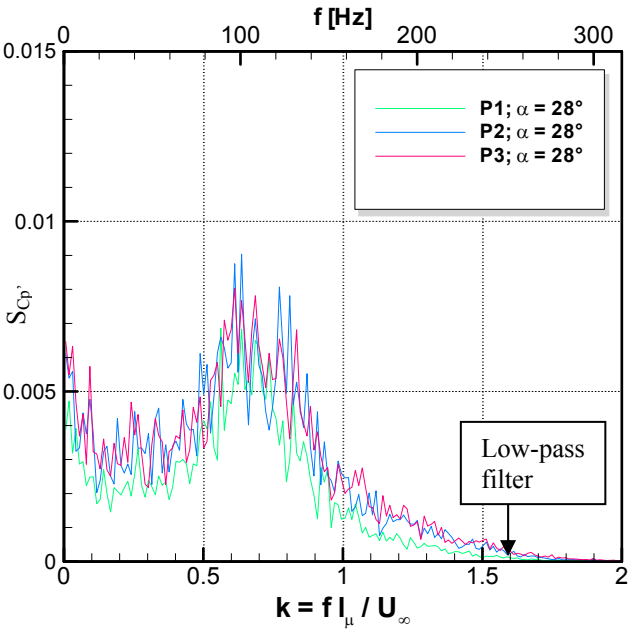

Fig. 12 Amplitude pressure spectra $S_{Cp'}$ taken at stations P1, P2, and P3 for $\alpha = 28°$; $Re_{l\mu} \approx 0.7 \times 10^6$.

4 Conclusions and Outlook

Detailed wind tunnel experiments have been conducted on an advanced trainer aircraft model to study the fin buffet flow environment. The low-speed tests are carried out for a Reynolds number based on the wing mean aerodynamic chord of $Re_{l\mu} = 0.68 \times 10^6$ ($M_\infty = 0.12$) and include angles of attack from $\alpha = 0°$ up to $\alpha = 30°$. The turbulent flow fields are measured using advanced hot-wire anemometry and small cross-wire probes while the unsteady fin surface pressures are recorded with miniature differential pressure transducers.

Main results are as follows:

1. The wing flow is dominated by leading-edge vortices shed already at low angles of attack. At the 45 deg swept wing, vortex bursting takes place over the wing subsequently of vortex formation, so that vortex breakdown is present from low to high angles of attack.
2. A strong leading-edge vortex emanates also from the air intake wing strake and combines with the burst wing vortex at moderate angle of attack.
3. The burst vortices exhibit a limited radial range of local turbulence maxima surrounding the strongly expanded vortex cores. This turbulence range approaches the aircraft symmetry plane with increasing angle of attack because the burst wing vortex is further enlarged while its axis is shifted inboard and upward.
4. The turbulence levels within the fin section as well as the fin pressure fluctuations increase significantly above $\alpha \approx 20°$ caused by induction effects of the highly turbulent flow region of the burst wing vortices. This effect becomes dominant when the distance between the fin surface and the inboard vortex shear layer is smaller than the vortex core radius. The rms pressures reach levels of about 9%-10% at maximum angle of attack.
5. Velocity and pressure spectra show characteristic narrow-band distributions indicating quasi–periodic fluctuations. They arise from the vortex breakdown flow which is subject to a helical mode instability of this swirling flow field with retarded axial core flow. Pressure spectra are affected above $\alpha \approx 22°$.
6. A universal frequency parameter can be derived for the dominant frequencies f_{dom} of the burst vortex velocity and pressure fluctuations. This frequency parameter is based on a length scale for the lateral expansion of the burst vortex core and a characteristic velocity given by the wing leading–edge normal velocity component.

Acknowledgments

The support of the investigations by the EADS Deutschland GmbH, Military Aircraft Systems (MAS-MEG6) is gratefully acknowledged.

References

[1] Bisplinghoff, R L, Ashley, H, and Halfman, R L. *Aeroelasticity*. Dover Publications, Mineola, New York, 1996

[2] Luber W, Becker J. The Role of Buffet in the Structural Design of Eurofighter Typhoon. AIAA Paper 2003–1889, April 2003.

[3] Breitsamter C. *Unsteady Aerodynamics*, Lecture Manuscript, Institute of Aerodynamics, Technische Universität München, 2008.

[4] Ferman, M A, Patel, S R, Zimmermann, N H, and Gerstenkorn, G. A Unified Approach to Buffet Response of Fighter Aircraft Empennage. *Aircraft Dynamic Loads due to Flow Separation*, AGARD–CP–483, Sorrento, Italy, April 1–6, 1990, pp. 2-1–2-18.

[5] Meyn, L A, and James, K D. Full–Scale Wind Tunnel Studies of F/A–18 Tail Buffet. *Journal of Aircraft*, Vol. 33, No. 3, 1996, pp. 589–595.

[6] Lee, B H K. Vertical Tail Buffeting of Fighter Aircraft. *Progress in Aerospace Sciences*, Vol. 36, No. 3–4, 2000, pp. 193–279.

[7] Sheta, E F, and Huttsell, L J. Numerical analysis of F/A–18 tail buffet. AIAA Paper 2001–1664, April 2001.

[8] Breitsamter C, and Laschka B. Fin Buffet Pressure Evaluation Based on Measured Flowfield Velocities, *Journal of Aircraft*, Vol. 35, No. 5, 1998, pp. 806–815.

[9] Breitsamter C. *Turbulente Strömungsstrukturen an Flugzeugkonfigurationen mit Vorderkantenwirbeln*. Dissertation, Technische Universität München, Herbert Utz Verlag Wissenschaft, 1997.

[10] Hummel D. On the Vortex Formation over a Slender Wing at Large Angles of Incidence, *High Angle of Attack Aerodynamics*, AGARD–CP–247, Sandefjord, Norway, Oct. 4–6, 1978, pp. 15-1–15-17.

[11] Hummel D. The Second International Vortex Flow Experiment (VFE-2): Objectives and Present Status. AIAA Paper 2007-4446, June 2007.

[12] Breitsamter, C. Unsteady Flow Phenomena Associated with Leading-Edge Vortices. *Progress in Aerospace Sciences*, Vol. 44, No. 1, 2008, pp. 48–65.

[13] Hummel D. Effects of Boundary Layer Formation on the Vortical Flow above Slender Delta Wings, *Enhancement of NATO Military Flight Vehicle Performance by Management of Interacting Boundary Layer Transition and Separation*, Prag, Czech Republic, 4–7 Oct 2004.

[14] Lambourne N C, and Bryer D W. The bursting of leading edge vortices. Some observations and discussion of the phenomenon, *ARC R & M 3282*, 1962.

[15] Hummel D. Untersuchungen über das Aufplatzen der Wirbel an schlanken Deltaflügeln, *Zeitschrift für Flugwissenschaften und Weltraumforschung*, Band 13, 1965, pp. 158–168.

[16] Gursul I. Unsteady Flow Phenomena over Delta Wings at High Angle of Attack, *AIAA Journal*, Vol. 32, No. 2, 1994, pp. 225–231.

[17] Gursul, I. Review of Unsteady Vortex Flows over Slender Delta Wings. *Journal of Aircraft*, Vol. 42, No. 2, 2005, pp. 299–319.

[18] Özgören, M, Sahin, B, and Rockwell, D. Perturbations of a Delta Wing: Control of Vortex Breakdown and Buffeting. *Journal of Aircraft*, Vol. 38, No. 6, 2001, pp. 1040–1050.

[19] Kim, Y, Rockwell, D, and Liakopoulos, A. Vortex Buffeting of Aircraft Tail: Interpretation via Proper Orthogonal Decomposition. *AIAA Journal*, Vol. 43, No. 3, 2005, pp. 550–559.

[20] Hebbar, S K, Platzer, M F, and Frink, W D. Effect of Leading-Edge Extension Fences on the Vortex Wake of an F/A–18 Model. *Journal of Aircraft*, Vol. 32, No. 3, 1995, pp. 680–682.

[21] Ashley H, Rock S M, Digumarthi R V, Chaney K, and Eggers Jr. A J. *Active Control for Fin Buffet Alleviation*, U.S. Air Force Wright Lab., WL-TR-93-3099, Wright-Patterson AFB, OH, Jan. 1994.

[22] Becker, J, and Luber, W. Comparison of Piezoelectric and Aerodynamic Systems for Aircraft Vibration Alleviation. *SPIE 5th Annual Symposium on Smart Structures and Materials*, Conference Paper 3326-04, San Diego, CA, March 1998.

[23] Galea, S C, Ryall, T G, Henderson, D A, Moses, R W, White, E V, and Zimcik, D G. Next Generation Active Buffet Suppression System. AIAA Paper 2003–2905, July 2003.

[24] Sheta, E. F.: Alleviation of Vertical Tail Buffeting of F/A–18 Aircraft. *Journal of Aircraft*, Vol. 41, No. 2, 2004, pp. 322–330.

[25] Breitsamter C. Aerodynamic Active Control for Fin-Buffet Load Alleviation, *Journal of Aircraft*, Vol. 42, No. 5, 2005, pp. 1252 – 1263.

Copyright Statement